Gas-phase electronic spectroscopy of nuclear spin isomer separated $H_2O@C$ and $D_2O@C$

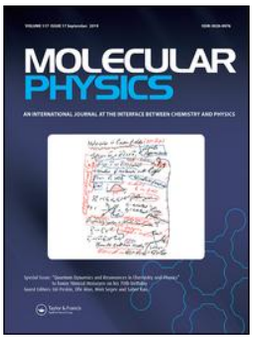

Taylor & Francis
Taylor & Francis Group

Molecular Physics

An International Journal at the Interface Between Chemistry and Physics

ISSN: (Print) (Online) Journal homepage: https://www.tandfonline.com/loi/tmph20

Gas-phase electronic spectroscopy of nuclear spin isomer separated $H_2O@C$ and $D_2O@C$

Johanna Rademacher, Elliott S. Reedy, Fabrizia Negri, Shamim Alom, Richard J. Whitby, Malcolm H. Levitt & Ewen K. Campbell

To cite this article: Johanna Rademacher, Elliott S. Reedy, Fabrizia Negri, Shamim Alom, Richard J. Whitby, Malcolm H. Levitt & Ewen K. Campbell (2023): Gas-phase electronic spectroscopy of nuclear spin isomer separated $H_2O@C$ and $D_2O@C$, Molecular Physics, DOI: 10.1080/00268976.2023.2173507

To link to this article: https://doi.org/10.1080/00268976.2023.2173507

MOLECULAR PHYSICS e2173507
https://doi.org/10.1080/00268976.2023.2173507

Taylor & Francis
Taylor & Francis Group

FESTSCHRIFT IN MEMORY OF DIETER GERLICH SPECIAL ISSUE

Gas-phase electronic spectroscopy of nuclear spin isomer separated $H_2O@C_{60}^+$ and $D_2O@C_{60}^+$

Johanna Rademacher[a], Elliott S. Reedy[a], Fabrizia Negri[c], Shamim Alom[b], Richard J. Whitby[b], Malcolm H. Levitt[b] and Ewen K. Campbell[a]

[a]School of Chemistry, University of Edinburgh, Edinburgh, UK; [b]Chemistry, University of Southampton, Southampton, Hants, UK; [c]Dipartimento di Chimica 'Giacomo Ciamician' and INSTM, Università di Bologna, Bologna, Italy

ABSTRACT

Gas-phase electronic spectra of $H_2O@C_{60}^+$ and $D_2O@C_{60}^+$ are presented. These data were obtained by one-photon dissociation of weakly bound helium complexes synthesised in a 3 K ion trap. Measurements were recorded in the vicinity of the ^2A_g,$^2B_g \leftarrow X\,^2A_u$ electronic transitions of the C_{60}^+ cage. Two-colour hole burning experiments enabled nuclear spin isomer pure data to be obtained. The spectra are rich in structure with many absorptions attributed to internal excitation of the encapsulated molecule accompanying the C_{60}^+ electronic transition. The experimental data are complemented with density functional theory calculations using the B3LYP functional and 6-31++G** basis set.

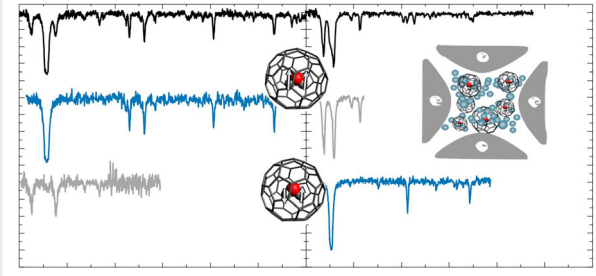

ARTICLE HISTORY
Received 29 November 2022
Accepted 18 January 2023

KEYWORDS
Electronic spectroscopy; endohedral fullerenes; cryogenic ion trapping; nuclear spin isomers

1. Introduction

Molecular surgery has enabled the synthesis of macroscopic quantities of endohedral C_{60} fullerenes that contain small molecules such as H_2 [1], H_2O [2, 3], HF [4] and CH_4 [5]. These developments have allowed experimental investigation into their unique properties. The endohedral of relevance to the present work is $H_2O@C_{60}$. The encapsulated water is an asymmetric top rotor and displays nuclear spin isomerism, with total nuclear spin $I = 1$ or $I = 0$, referred to as *ortho* and *para*, respectively. The *ortho* isomer is threefold degenerate while *para* is non-degenerate, resulting in a 3:1 *ortho*:*para* ratio in the high-temperature limit. As protons are fermions, the Pauli principle dictates that the overall wave function ($\Psi_{tot} = \Psi_e\Psi_v\Psi_r\Psi_{ns}$) is antisymmetric with respect to exchange of the two H-nuclei. In the gas phase, *ortho* and *para* H_2O do not readily interconvert allowing experiments to reveal differences in their chemical reactivity [6].

A consequence of nuclear spin statistics is the connection between the symmetry of rotational (Ψ_r) and nuclear spin (Ψ_{ns}) wavefunctions. The rotations of an asymmetric top are denoted $J_{K_aK_c}$, where K_a and K_c are projections in the prolate and oblate symmetric top limits. In the lowest vibrational level of the ground electronic state of gas-phase water and $H_2O@C_{60}$ [7–9], the *ortho* nuclear spin isomer is associated with $K_a + K_c =$ odd levels and *para* with $K_a + K_c =$ even. These combinations can switch if the symmetry of one of the other contributing parts of the total wavefunction is changed,

CONTACT Ewen K. Campbell e.k.campbell@ed.ac.uk School of Chemistry, University of Edinburgh, Joseph Black Building, Kings Buildings, David Brewster Road, Edinburgh EH9 3FJ, UK

Supplemental data for this article can be accessed here. https://doi.org/10.1080/00268976.2023.2173507

which happens, for example, when odd quanta of the asymmetric stretching mode of H_2O are excited [7] and upon ionisation to the ground state of H_2O^+ [10].

Rotational transitions of the encapsulated H_2O in $H_2O@C_{60}$ have been observed with IR [7], THz spectroscopy [11, 12] and inelastic neutron scattering [8, 9]. The experimental results resemble the rotational pattern of free H_2O but the surrounding cage affected the rotational constants of H_2O [7]. Furthermore, in the solid phase, the degeneracy of the rotational 1_{01} *ortho* ground state of H_2O is lifted due to crystal field effects [8, 9, 13, 14]. By observing the intensity change of the rotational transitions in the condensed phase it was possible to show that slow spin forbidden *ortho*↔*para* interconversion takes place and to assign the transitions to the different spin isomers [7, 8]. A change in dielectric constant was also observed upon ortho–para conversion [15]. The decreased intensity of transitions originating from 1_{01} was confirmed by a loss of NMR signal, because of the NMR-inactivity of the *para* spin isomer [15, 16].

The carbon cage resembles a spherical potential around H_2O which is subject to strong quantum effects [17, 18]. For example, the confinement is responsible for the quantisation of H_2O translational modes [7, 11, 12]. Additionally, computational work [19] predicts frustrated vibrations and rotations, which are yet to be observed in experiments. However, there are features observed in THz spectroscopy [11] attributed to hot bands based on temperature-dependent experiments [12] but these remain unassigned to particular translational or rotational motions. The dipole moment of the H_2O molecule is also shielded significantly by the C_{60} surrounding [15, 19, 20].

The influence of H_2O on the cage has also been studied [21, 22] and the UV-Vis spectrum of $H_2O@C_{60}$ showed negligible difference to the electronic transition(s) of the empty cage in solution [2]. ^{13}C NMR studies of the endohedral showed no reduced symmetry of the cage in $H_2O@C_{60}$ [23]. However, the singly charged cation $H_2O@C_{60}^+$ has not been thoroughly investigated yet. As C_{60}^+ is an open shell system, it is expected to show more significant interactions between the encapsulated molecule and the surrounding carbon cage. In this contribution, gas-phase electronic spectra of $H_2O@C_{60}^+$ are presented and contrasted to that of C_{60}^+ [24]. The data were obtained using He tagging at cryogenic temperatures. The contributions of *para* and *ortho* H_2O are separated by two-colour hole burning experiments. The assignment of features in the spectra is supported by DFT calculations.

Sections 2 and 3 describe the experimental and computational methods employed, respectively. Section 4 contains the electronic spectra of $H_2O@C_{60}^+$ and $D_2O@C_{60}^+$ and a discussion of the observed transitions along with their proposed assignments, while conclusions are given in Section 5.

2. Experimental

The $H_2O@C_{60}$ sample was synthesised following a synthetic route known as 'molecular surgery' [2, 3]. A few mg of 80 % filled $H_2O@C_{60}$ ($D_2O@C_{60}$) were heated in an oven to $\sim 350^\circ$ C. Singly charged parent ions were produced from the neutral gas using electron impact at 40 eV. The experiments were carried out using the apparatus described in detail in Refs. [25, 26], and only the parameters specific to the present work are given here.

In ion trapping experiments, species with m/z below 738 (740) were removed using the first quadrupole mass spectrometer. The nominal trap temperature was 4 K and the He buffer gas number density was 10^{15} cm^{-3}. These low trap temperatures and high He number densities, coupled with long interaction times (several hundred ms), allow $H_2O@C_{60}^+{-}He_n$ ($D_2O@C_{60}^+{-}He_n$) complexes to form, which can be seen in Figure 1. For example, to generate the spectrum in Figure 1, $H_2O@C_{60}^+$ cations were loaded into the trap for 200 ms by lowering the potential applied to the axial entrance electrode. During the first 500 ms they interact with helium buffer gas, which was subsequently pumped out for 420 ms before the trap contents were extracted and analysed by the second quadrupole mass spectrometer. The trapping process was repeated at a repetition rate of 1 Hz.

Photofragmentation spectra of $H_2O@C_{60}^+{-}He$ ($D_2O@C_{60}^+{-}He$) were recorded by irradiation of the ion cloud with a continuous wave Ti:Sap laser for 30 ms at the end of the trapping cycle. The irradiation time was controlled by use of a mechanical shutter. The mass-channel of the $H_2O@C_{60}^+{-}He$ ($D_2O@C_{60}^+{-}He$) complexes with $m/z = 742$ (744) is monitored on alternating cycles with (N_i) and without (N_0) exposure to the radiation to obtain the depletion of complexes as a function of the laser frequency and account for fluctuations in the number of stored ions. For the two-colour experiments, a second near-infrared CW laser (diode) was used to continuously irradiate the ions during the entire trapping cycle at a fixed (resonant) frequency. This enabled the depletion of ions belonging to one nuclear spin isomer. In this case, the number of $H_2O@C_{60}^+{-}He_n$ ($D_2O@C_{60}^+{-}He_n$) complexes remaining in the trap following exposure to both (N_i) lasers or only the diode laser (N_0) were monitored to reveal nuclear spin isomer pure spectra.

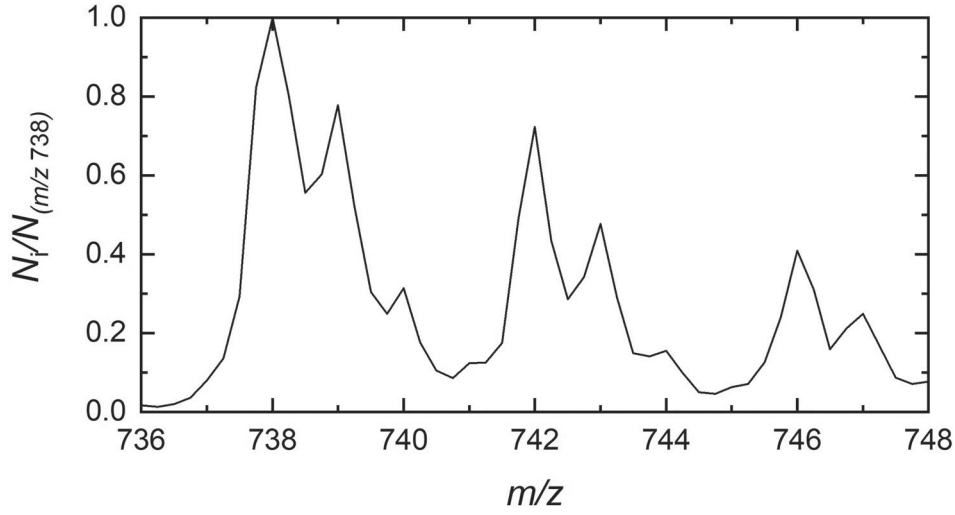

Figure 1. Mass spectrum recorded after storage of $H_2O@C_{60}^+$ in helium buffer gas at 4 K.

3. Computational

The equilibrium structure of $H_2O@C_{60}^+$ was determined with density functional theory in the unrestricted formalism, using the B3LYP functional and the 6-31++G** basis set. The B3LYP functional was selected for these calculations owing to its generally good performance for large conjugated systems and specifically because it was previously employed to study C_{60}^+ [27], in conjunction with its generally smaller spin contamination compared to hybrid functionals with larger contributions of HF exchange [28]. In addition, weak dispersion-like intra- and inter-molecular noncovalent interactions were included via the D3(BJ) correction term [29–31]. An integral accuracy cutoff of 10^{-12} in combination with an ultrafine integration grid were requested during the Hessian calculations. Geometry optimisation and vibrational frequency calculations were carried out using the Gaussian16 suite of programs [32]. Gaussian16 evaluates the molecular Hessian in Cartesian coordinates, and the vibrational frequencies of any isotopically substituted species may therefore easily be obtained on the basis of the full Hessian by changing the atomic masses. The vibrational frequencies for $D_2O@C_{60}^+$ were then correlated with those of $H_2O@C_{60}^+$ by computing the Duschinsky rotation matrix for the two sets of vibrational normal modes [33]. The optimised geometry displayed a modest spin contamination, with a final value of S^2 resulting in 0.7539. The nature of the stationary point was assessed by vibrational frequency calculations that resulted to be all real. The final $H_2O@C_{60}^+$ structure has no symmetry elements and is slightly distorted from C_{2v}, with the two OH bond lengths being 0.965 and 0.966 Å and the HOH angle measuring 104.9°.

4. Results and discussion

4.1. Electronic spectrum of $H_2O@C_{60}^+$: comparison with C_{60}^+

The gas-phase electronic spectrum of C_{60}^+ below 10 K is presented in Figure 2 in comparison to that of $H_2O@C_{60}^+$. The former shows two intense bands at 10,378 and 10,438 cm^{-1} and two weaker absorptions at 10,603 and 10,674 cm^{-1}. The two intense features were assigned to the origin bands of the $^2B_g \leftarrow \tilde{X}\,^2A_u$ and $^2A_g \leftarrow \tilde{X}\,^2A_u$ electronic transitions of C_{60}^+ based on calculations, which predicted a Jahn–Teller distortion of the C_{60}^+ cage [27]. The lowest energy vibrational mode ($\sim$230 cm^{-1}) of C_{60}^+ in the ^2B_g and ^2A_g states causes the bands at 10,603 and 10,674 cm^{-1}. Comparison of the electronic spectra shown in Figure 2 suggests that only one electronic transition is observed in the $H_2O@C_{60}^+$ spectrum instead of the two observed for C_{60}^+. The strongest absorption feature of $H_2O@C_{60}^+$ appears at 10,429 cm^{-1}, which lies between the two C_{60}^+ origin bands.

Additionally, the $H_2O@C_{60}^+$ spectrum shows several less prominent features with varying intensities close to 10,429 cm^{-1}. The energy separation between the observed bands with respect to the strongest absorption is between 9 and 250 cm^{-1}. Most of these fall below the lowest frequency cage vibration and are also too low in energy to be associated with vibrational modes of (free) H_2O. However, these energy separations are suggestive of rotational levels of gas-phase H_2O or translational modes associated with confinement in the cage, which were observed in $H_2O@C_{60}$ [7]. These features of the $H_2O@C_{60}^+$ spectrum indicate that excitations of the encapsulated H_2O molecule may accompany the electronic transition of the C_{60}^+ cage. The calculations

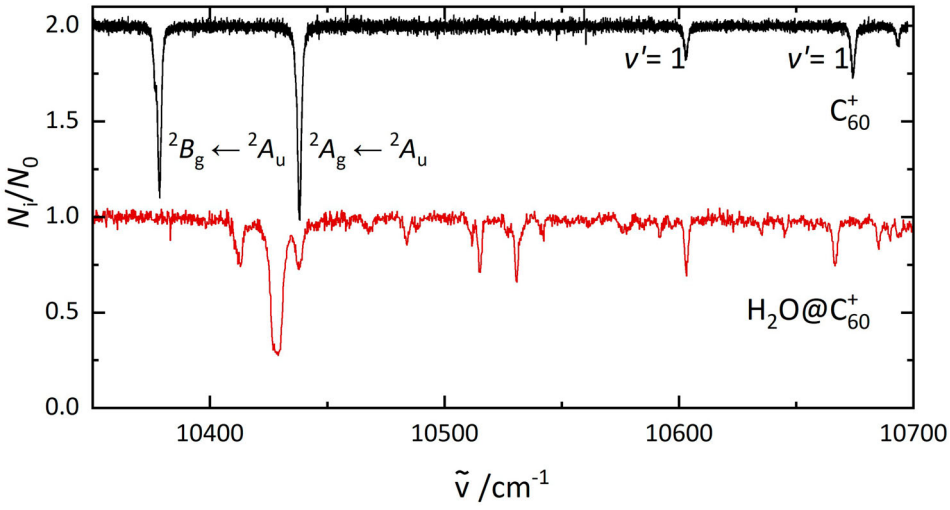

Figure 2. The electronic spectrum of C_{60}^+ (top) and $H_2O@C_{60}^+$ (bottom), recorded under the same laboratory conditions. The data are photofragmentation spectra of C_{60}^+—He and $H_2O@C_{60}^+$—He complexes.

Table 1. Vibrational and translational modes obtained from calculations.

	B3LYP/6-31++G**	
Mode	$H_2O@C_{60}^+$	$D_2O@C_{60}^+$
T_1/cm^{-1}	125	115
T_2/cm^{-1}	126	120
T_3/cm^{-1}	128	119
ν_1/cm^{-1}	111	80
ν_2/cm^{-1}	101	73
ν_3/cm^{-1}	34	26

reported here indicate that similar energy separations to those observed in the experimental spectrum are expected for vibrational and translational modes of H_2O in the ground electronic state of $H_2O@C_{60}^+$, as presented in Table 1.

Note that although these experiments are carried out on weakly bound $H_2O@C_{60}^+$—He complexes, the exohedral helium is expected to be a minor perturbation to the electronic transitions of $H_2O@C_{60}^+$, as was the case for C_{60}^+ (see supplementary information). The following discussion and assignment of the rich spectrum is made on this basis and the assumption that the exohedral, weakly bound, helium atom does not affect the symmetry of Ψ_e.

4.2. Ortho/para ratio

More information on the cause of the band pattern can be gained by observations of the absolute number of complexes depleted following irradiation on resonance because the broad width of the 10,429 cm^{-1} band in the electronic spectrum shown in Figure 2 indicates saturation. Even with a high laser fluence, a significant number of complexes remained in the trap after irradiating them at 10,438 cm^{-1}, as indicated in Figure 3. It was observed that the number of remaining ions varied depending on the particular transition excited.

The conversion between nuclear spin states is forbidden and takes several hours in the condensed phase [8, 16]. In our gas phase experiment, the high spin temperature *ortho*/*para* ratio is expected to be conserved. This is consistent with the data shown in Figure 3, where 73±5% ions do not interact with the laser at 10,438 cm^{-1}. The 27±5% that absorb at this energy are therefore attributed to *para* $H_2O@C_{60}^+$.

4.3. Separation of ortho and para nuclear spin isomers by 2 colour experiments

As it was possible to remove one group of nuclear spin isomers from the trap, a two-colour setup was used to record nuclear spin isomer pure electronic spectra. These are presented in Figure 4. The spectra were assigned to *ortho* and *para* based on the fraction of ions that were depleted. The *ortho* spectrum shows one intense transition at 10,429 cm^{-1}, two bands at 10,515 and 10,530 cm^{-1}, one band at 10,603 cm^{-1}, and one more at 10,666 cm^{-1}. Four bands of *para* $H_2O@C_{60}^+$ were observed, all at energies below 10,500 cm^{-1}.

4.4. Assignment of the absorption features

To allow assignment of the bands in the spectrum, the energy differences between the band at 10,429 cm^{-1} and the others are compared to the rotational energy levels of free water. The three transitions from the *ortho* and *para* rotational ground state are $1_{10} \leftarrow 1_{01}$, $1_{11} \leftarrow 0_{00}$ and $2_{12} \leftarrow 1_{01}$. The energy separation between these

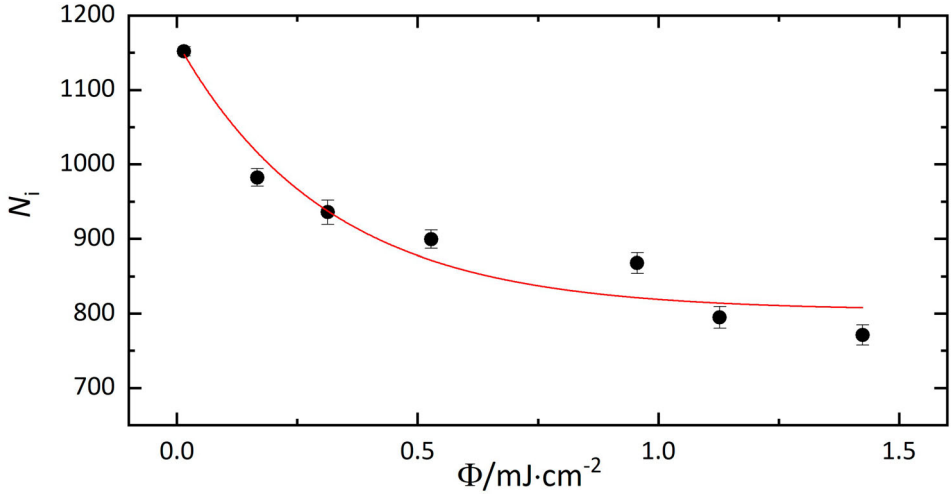

Figure 3. Number of $H_2O@C_{60}^+$—He complexes (N_i) as a function of laser fluence upon irradiation at 10,438 cm^{-1}. Without exposure to laser radiation, 1100±60 ions with $m/z = 742$ were in the trap. 800±30 complexes remain after irradiation, corresponding to 73±5% of the population.

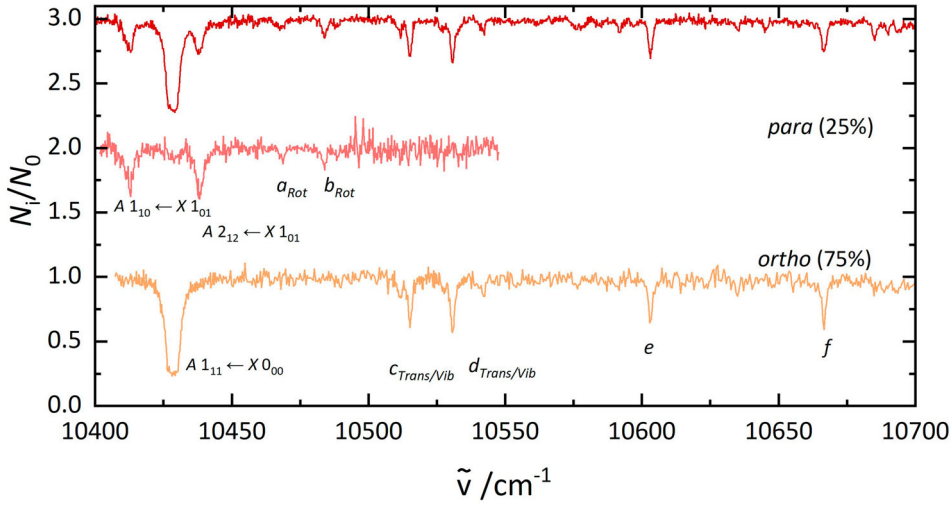

Figure 4. Electronic spectra of $H_2O@C_{60}^+$ (top), *p*-$H_2O@C_{60}^+$ (middle), and *o*-$H_2O@C_{60}^+$ (bottom). The lower two traces were obtained in 2 colour experiments. The middle spectrum was recorded by fragmenting all complexes that absorb at 10,429 cm^{-1}. The bottom spectrum was recorded after irradiation at 10,438 cm^{-1}.

transitions resembles the pattern observed for $H_2O@C_{60}^+$, as shown in Figure 5. Alternative explanations involving hot bands or Q-branch transitions were explored but do not agree with the observed energy separations.

To aid the assignment, simulations of H_2O electronic transitions have been carried out using H_2O rotational constants provided by calculations on $H_2O@C_{60}^+$. These simulations, which ignore any effects of the C_{60}^+ cage, have been carried out using PGopher software [34] in C_{2v} symmetry. Based on the observed nuclear spin isomer ratios, the spin temperature was set to 300 K (high-temperature limit). B_2 electronic symmetry in the ground and excited electronic state resulted in an intensity pattern in agreement with the experiments. A rotational temperature of 5 K and full width half maximum (FWHM) of 2.5 cm^{-1} were used. The $A\,0_{00} \leftarrow X\,0_{00}$ energy was chosen in order to match the $A\,1_{11} \leftarrow X\,0_{00}$ transition to the 10,429 cm^{-1} band of the experimental spectrum. Figure 5 shows the resemblance of the three lowest energy bands in $H_2O@C_{60}^+$ with the simulated spectrum using rotational levels of free H_2O (middle trace). While these results are in qualitative agreement, they can be improved when a geometry change between the ground and excited state is considered.

A simulated electronic spectrum involving a geometry change of H_2O between the ground and excited state is shown in the upper trace of Figure 5. The rotational constant C_A of the excited state can be derived directly from the experimental spectrum [35]. Furthermore, the fitting capability of the PGopher software was used to extract

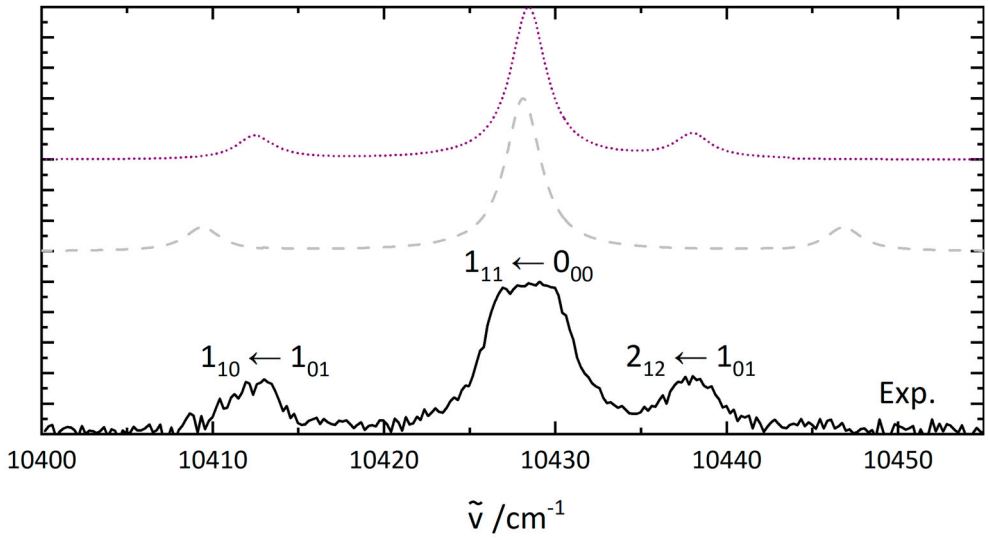

Figure 5. PGopher simulations of the rotational pattern of an electronic transition of H_2O. The details of the simulations are explained in the text. The middle trace uses the parameters based on a geometry optimisation (B3LYP/6-31++G**) while the upper one shows a fit involving a geometry change of H_2O between ground and excited state.

Table 2. Rotational constants used for the simulation in Figure 5.

Constant	$H_2O@C_{60}^+$ /cm^{-1}	$D_2O@C_{60}^+$/cm^{-1}
ΔE	10,394.83*	10,412.15*
A_X	27.25	13.63
B_X	14.25	7.13
C_X	9.36	4.68
A_A	27.25	11*
B_A	13.98*	5.38*
C_A	6.35*	2.75*

Notes: Values without * are taken from the optimised geometry. * indicates free parameters that were obtained during the fit. Subscript $_X$ and $_A$ refer to the ground and excited state, respectively.

the rotational constant B_A for the excited state, and the $A\,0_{00} \leftarrow X\,0_{00}$ energy. This fit used the calculated constants of H_2O in $H_2O@C_{60}^+$ in the ground states as inputs, together with $A_X = A_A$. The constants used to obtain Figure 5 are listed in Table 2.

The proposed assignment indicated in Figure 5, with the 10,429 cm^{-1} absorption originating from the 0_{00} level, coupled with the observation that the associated nuclear spin isomer is responsible for 75% of the total population, implies that even $K_a + K_c$ are *ortho* in $H_2O@C_{60}^+$ (or $H_2O@C_{60}^+$–He). This differs from $H_2O@C_{60}$, where even $K_a + K_c$ rotational functions are associated with the *para* nuclear spin isomer, suggesting that the $H_2O@C_{60}^+$ (or $H_2O@C_{60}^+$–He) electronic wave function is antisymmetric. This interpretation is reached because the Pauli principle requires the overall wavefunction to be antisymmetric with respect to exchange of the two H-nuclei. As the transition does not originate from a vibrationally excited level, Ψ_e is the contributor to $\Psi_{tot} = \Psi_e\Psi_v\Psi_r\Psi_{ns}$ that differs between H_2O and $H_2O@C_{60}^+$ ($H_2O@C_{60}^+$–He) for the same rotational and nuclear spin states.

There are several possibilities for assignment of the bands to a higher energy than the three shown in Figure 5. For example, the constants derived from the simulation lead to a near coincidence in energy for the 10,484 cm^{-1} (***b***) absorption with an $A\,2_{21} \leftarrow X\,1_{10}$ transition (10,483 cm^{-1}) or the 10,469 cm^{-1} (***a***) absorption, when the A rotational constant changes by ~ 20% between ground and excited state, which is observed for the other rotational constants. This hot band transition, however, is ruled out due to the absence of absorption to lower energy than 10,396 cm^{-1} which would be expected to be observed for the $A\,1_{01} \leftarrow X\,1_{10}$ transition. Therefore it appears that H_2O inside the C_{60}^+ cage is rotationally cold in our experiment.

Band ***b*** is also close to the predicted $A\,3_{03} \leftarrow X\,1_{01}$ (10,482 cm^{-1}) and $A\,2_{21} \leftarrow X\,1_{01}$ transition (10,500 cm^{-1}). The latter transition depends on A_A and could also appear at 10,484 cm^{-1} if the value for A_A varies in a reasonable %-range after electronic excitation (i.e. comparable to the other rotational constants). Here the value for the excited state rotational constant would be 22 cm^{-1} with a 10,400 cm^{-1} $A\,0_{00} \leftarrow X\,0_{00}$ energy, which is similar to the constants for the excited vibrational level in neutral $H_2O@C_{60}$ (23.15 cm^{-1}) [7]. A change of A_A would require a slight adjustment of the origin energy to maintain the agreement in energy with the previously assigned bands, but would otherwise not influence the shape of the spectrum. However, the $A\,2_{21} \leftarrow X\,1_{01}$ transition is not a dipole-allowed transition of asymmetric top rotors and the $A\,3_{03} \leftarrow X\,1_{01}$ has $\Delta J = 2$.

The $A\,2_{20} \leftarrow X\,1_{01}$ and $A\,2_{11} \leftarrow X\,1_{01}$ transitions are also in the same energy region and are expected to have an energy of 10,489 and 10,460 cm^{-1} if $A_A = 22\,cm^{-1}$. These are *a* and *c*-type transitions, respectively, while all the other assigned features are *b*-type. A component of the transition dipole along these axes would be required for such nuclear spin forbidden features.

The only transition below 10,500 cm^{-1} in the spectrum of *ortho*-$H_2O@C_{60}^+$ is assigned to $A\,1_{11} \leftarrow X\,0_{00}$. The higher energy bands ***c*** and ***d*** at 10,515 and 10,531 cm^{-1} lie 119 and 135 cm^{-1} from the predicted $A\,0_{00} \leftarrow X\,0_{00}$ energy. Previous DFT calculations [19] at the PBEO/6-311++G** level of theory indicated that frustrated vibrations and translations of water inside neutral C_{60} could be observed. In DFT (B3LYP/6-311++G**) calculations of the charged $H_2O@C_{60}^+$ system, three translational modes between 125 and 128 cm^{-1} and three frustrated vibrational modes (34, 101 and 111 cm^{-1}) were found in the electronic ground state. Therefore the bands ***c*** and ***d*** are consistent with the excitation of either a frustrated vibrational mode or with translations that are quantised due to the spacial confinement. Translations have also been observed experimentally at 110 cm^{-1} in $H_2O@C_{60}$ [7], which is similar to the energy inferred here. Based on these computational results, it seems plausible that the bands ***c*** and ***d*** could be due to either quantised translations or frustrated vibrations.

The 10,603 and 10667 cm^{-1} absorptions, ***e*** and ***f***, have an energy separation of 206 and 270 cm^{-1} from $A\,0_{00} \leftarrow X\,0_{00}$, which is close to the $\sim$230cm^{-1} energy of the C_{60}^+ cage vibration. The $\sim$270 cm^{-1} energy separation of absorption ***f*** also corresponds to twice the energy separation of band ***d*** with respect to the $A\,0_{00} \leftarrow X\,0_{00}$ energy. These two bands could therefore be caused by the excitation of two quanta of the same vibration or translation. A summary of the potential assignments is given in Table 3.

Table 3. Absorption energies and proposed assignment of bands in the $H_2O@C_{60}^+$ and $D_2O@C_{60}^+$ spectra.

$H_2O@C_{60}^+$	$\tilde{\nu}$/cm^{-1}	$D_2O@C_{60}^+$	$\tilde{\nu}$/cm^{-1}	Assignments	
	10,412		10,418	Rot	($A\,1_{10} \leftarrow X\,1_{01}$)
	10,429		10,426	Rot	($A\,1_{11} \leftarrow X\,0_{00}$)
	10,438		10,429	Rot	($A\,2_{12} \leftarrow X\,1_{01}$)
a	10,469	I	10,447	Rot	($A\,2_{21} \leftarrow X\,1_{10}$)
					($A\,2_{11} \leftarrow X\,1_{01}$)
b	10,484	II	10,457	Rot	($A\,2_{21} \leftarrow X\,1_{10}$)
					($A\,2_{21} \leftarrow X\,1_{01}$)
					($A\,3_{03} \leftarrow X\,1_{01}$)
					($A\,2_{20} \leftarrow X\,1_{01}$)
c	10,516	III_a	10,502	Tr/Vib	
d	10,531	III_b	10,513	Tr/Vib	
		IV	10,506	Vib	
e	10,603	V	10,571	Vib	
f	10,666		–	Cage	

Notes: There are several possible assignments for bands ***a-f*** . See the text for a discussion.

4.5. Electronic spectrum of $D_2O@C_{60}^+$: comparison with $H_2O@C_{60}^+$

Further experiments on $D_2O@C_{60}^+$ were performed to support the assignments of the bands in the $H_2O@C_{60}^+$ electronic spectrum. Figure 6 shows the spectrum of $D_2O@C_{60}^+$ recorded under similar conditions to those used for $H_2O@C_{60}^+$. The intensity pattern of the bands is significantly different from the observations in $H_2O@C_{60}^+$, and the energy separations between the bands are smaller as expected due to the isotope effect. After irradiation at 10,418 cm^{-1}, 37±3% of the complexes remain in the trap while at 10,425 cm^{-1}, 63±3%

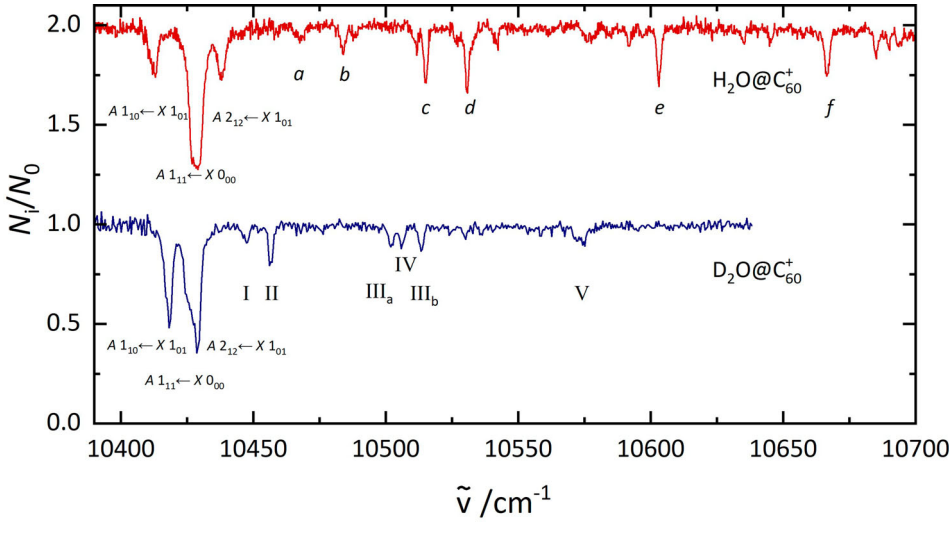

Figure 6. A comparison of the electronic spectrum of $H_2O@C_{60}^+$ (top) and $D_2O@C_{60}^+$ (bottom) recorded under similar laboratory conditions. The labels are discussed in the text.

of the complexes remain. These values correspond well to the 2:1 *o*/*p* ratio of D_2O observed in the high-temperature limit, as expected from the $H_2O@C_{60}^+$ experiment.

Substitution of H with D in $H_2O@C_{60}^+$ affects vibrations, rotations and translations of the encapsulated molecule differently. In D_2O an energy of $\frac{1}{\sqrt{2}}$ of the same H_2O vibrational mode would be expected. The rotational constants of D_2O are lower than those of H_2O by about a factor of 2, if both molecules have the same geometry. In translations, motion of the whole molecule in the constrained environment is involved, and the effect of the isotope substitution is less severe. Translations of D_2O would have $\sqrt{\frac{m_{H_2O}}{m_{D_2O}}}$ times the energy of those of H_2O [36].

4.6. Confirmation of assignment(s) based on isotope effect

To confirm the assignment of the lowest energy rotational transitions in $H_2O@C_{60}^+$, the same rotational transitions were simulated for $D_2O@C_{60}^+$. The results are shown in Figure 7 and the constants are listed in Table 2. Values of the rotational constants in the ground state were $\frac{1}{2}$ of those used for the simulation of H_2O, and the $A\,0_{00} \leftarrow X\,0_{00}$ energy was changed accordingly. The excited state rotational constants were obtained from PGopher fits. The good agreement between the simulation and the experimental results appears to support the previous assignment of the rotational transitions in $H_2O@C_{60}^+$. Two-colour spectra of $D_2O@C_{60}^+$ are shown in Figure 8.

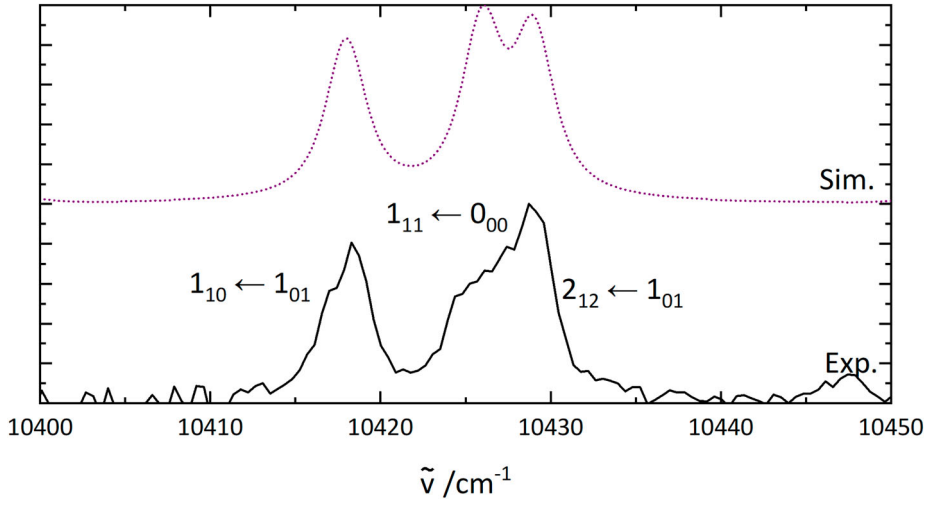

Figure 7. PGopher simulations of the rotational pattern of an electronic transition of D_2O in comparison with the experimental results on $D_2O@C_{60}^+$ (bottom). The rotational constants for the simulation are derived as described in the text.

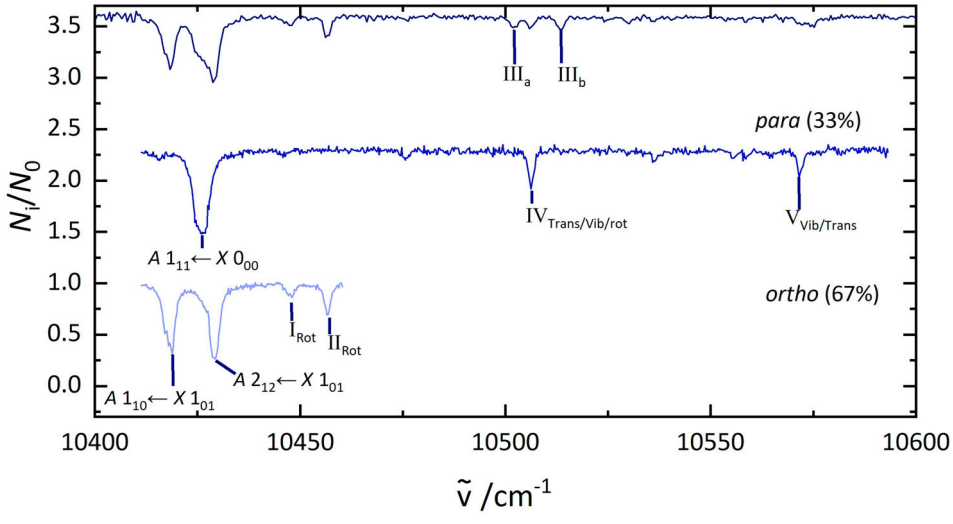

Figure 8. Electronic spectra of $D_2O@C_{60}^+$ (top), *para*-$D_2O@C_{60}^+$ (middle), and *ortho*-$D_2O@C_{60}^+$ (bottom). The middle trace was recorded by fragmenting all complexes that absorb at 10,418 cm^{-1} and the bottom trace was recorded by irradiating at 10,426 cm^{-1}.

The simulation has some further implications for the interpretation of the spectra and the structure of the two molecules. The experimentally derived C_A of the excited state of $D_2O@C_{60}^+$ has a value of 2.7 cm^{-1}. This is smaller than the 3.2 cm^{-1} which would be expected from $\frac{1}{2}C_A$. This indicates that the geometries of $H_2O@C_{60}^+$ and $D_2O@C_{60}^+$ are slightly different or that centrifugal distortion also contributes.

Another consequence of the simulation is that the $A\,0_{00} \leftarrow X\,0_{00}$ energy varies between the different isotopologues. Based on the assignments it is possible to estimate the energy for $A\,0_{00} \leftarrow X\,0_{00}$. This energy (10,409 cm^{-1}) is around 13 cm^{-1} higher than the estimated $A\,0_{00} \leftarrow X\,0_{00}$ of $H_2O@C_{60}^+$ at 10,396 cm^{-1}. It is assumed that differences in zero-point energies cause the blue shift of the $A\,0_{00} \leftarrow X\,0_{00}$ energy of $D_2O@C_{60}^+$ with respect to $H_2O@C_{60}^+$.

Based on the energy separations between the calculated $A\,0_{00} \leftarrow X\,0_{00}$ energy and the other bands in $H_2O@C_{60}^+$, the corresponding rotation, translation and vibrational modes expected to be seen in measurements on $D_2O@C_{60}^+$ could be estimated. The prediction can be compared to the experimental spectrum, to identify bands associated with translational, vibrational or rotational excitation.

In $H_2O@C_{60}^+$, the bands marked as ***a*** and ***b*** lie 74 and 89 cm^{-1} from $A\,0_{00} \leftarrow X\,0_{00}$. When dividing these energy separations by two and adding these values to the $A\,0_{00} \leftarrow X\,0_{00}$ transition of $D_2O@C_{60}^+$, the corresponding rotational levels in $D_2O@C_{60}^+$ are predicted at 10,444 and 10,452 cm^{-1}. The two observed bands at 10,447 and 10,453 cm^{-1} in $D_2O@C_{60}^+$ indicate that the bands at ***a*** and ***b*** are caused by rotational transitions of the encapsulated H_2O molecule and, based on the isomer separation, that these transitions are excited from the $X\,1_{01}$ rotational level. As described for $H_2O@C_{60}^+$, several forbidden rotational transitions are in a similar energy range, as presented in Table 3, but it can not be concluded which of these transitions is observed. However, it can be ruled out that these bands are due to translations or vibrations based on the predictions for $D_2O@C_{60}^+$.

Bands ***c*** and ***d*** are observed in the spectrum of the *ortho* isomer of $H_2O@C_{60}^+$. Rotational transitions are excluded from the possible explanations because there are no corresponding bands in $D_2O@C_{60}^+$. However, predicted translational (10,521 and 10,535 cm^{-1}) and vibrational transitions (10,493 and 10,503 cm^{-1}), present two options for assignment. Bands $\mathbf{III}_a$ and $\mathbf{III}_b$ in $D_2O@C_{60}^+$ are in a similar energy range but are not observed, as expected, in the *para* spectrum of $D_2O@C_{60}^+$. On the other hand band **IV** at 10,506 cm^{-1} is a close match to the predicted vibration at 10,504 cm^{-1} of *para*-$D_2O@C_{60}^+$ (band ***d*** in $H_2O@C_{60}^+$).

Considering the isotope effect for band ***e***, the equivalent vibration in $D_2O@C_{60}^+$ would show at 10,555 cm^{-1} and the rotation at 10,513 cm^{-1}. The predicted vibration is 15 cm^{-1} lower than the observed band **V** and the rotation is also close to band **IV** in $D_2O@C_{60}^+$, so it cannot be unambiguously assigned.

In the $H_2O@C_{60}^+$ electronic spectrum the band ***f*** at 10,666 cm^{-1} is close to the energy expected for the C_{60}^+-cage vibration. The measurement for $D_2O@C_{60}^+$ only covered an energy range up to 10,650 cm^{-1}. If this band is caused by a vibrational mode of the C_{60}^+ cage the effect of the isotopes would be minimal and then it would show at similar energies for both isotopologues when including the blue shift of the $A\,0_{00} \leftarrow X\,0_{00}$ energy for $D_2O@C_{60}^+$.

A summary of the above assignment discussion is presented in Table 3. The three lowest energy bands along with ***a*** and ***b*** can be classified as rotational transitions. The three bands in $D_2O@C_{60}^+$ $\mathbf{III}_a$, **IV** and $\mathbf{III}_b$ are only separated by a few wavenumbers and it is therefore difficult to assign them with certainty. Especially because band $\mathbf{III}_a$ and $\mathbf{III}_b$ of $D_2O@C_{60}^+$ do not correspond to bands with the same rovibronic symmetry in $H_2O@C_{60}^+$, they could also be caused by transitions not observed in $H_2O@C_{60}^+$.

5. Conclusion

Electronic spectra of $H_2O@C_{60}^+$ and $D_2O@C_{60}^+$ were recorded in the gas phase at temperatures below 10 K in the vicinity of the near-IR C_{60}^+ electronic transitions by photodissociation of weakly bound He complexes. Two-colour experiments allowed the removal of one nuclear spin isomer from the trap, allowing spin isomer pure spectra of these species to be obtained. The *ortho/para* ratio determined spectroscopically agrees with the high-temperature limit. The rich spectra obtained include contributions assigned to rotational excitation of the encapsulated H_2O (D_2O) molecules that appear to be relaxed to their ground states by buffer gas cooling in the trap. In contrast to C_{60}^+, only one of the two expected electronic transitions in this region was observed for the endohedral cations.

While not all of the observed spectral features have been assigned, the comparison of $D_2O@C_{60}^+$ and $H_2O@C_{60}^+$ spectra make it possible to exclude certain explanations and narrow down the possible assignments. For example, the isotope effect shows that there are more rotational transitions observed than the three allowed transitions from the rotational ground state of H_2O (D_2O). The results also imply that some of these bands could be caused by frustrated vibrational modes of the encapsulated molecule, which are yet to be observed in experiments on $H_2O@C_{60}$ or $H_2O@C_{60}^+$.

Disclosure statement

No potential conflict of interest was reported by the author(s).

Funding

The authors acknowledge financial assistance from the Royal Society [grant numbers RGF/EA/181035, URF/R1/180162] and Engineering and Physical Sciences Research Council [grant numbers EP/M001962/1, EP/P009980/1 and EP/T004 320/1].

References

[1] K. Komatsu, M. Murata and Y. Murata, Science **307**, 238 (2005). doi:10.1126/science.1106185
[2] K. Kurotobi and Y. Murata, Science **333**, 613 (2011). doi:10.1126/science.1206376
[3] A. Krachmalnicoff, M.H. Levitt and R.J. Whitby, Chem. Commun. **50**, 13037 (2014). doi:10.1039/C4CC06198E
[4] A. Krachmalnicoff, R. Bounds, S. Mamone, S. Alom, M. Concistrè, B. Meier, K. Kouřil, M.E. Light, M.R. Johnson, S. Rols, A.J. Horsewill, A. Shugai, U. Nagel, T. Rõõm, M. Carravetta, M.H. Levitt and R.J. Whitby, Nat. Chem. **8**, 953 (2016). doi:10.1038/nchem.2563
[5] S. Bloodworth, G. Sitinova, S. Alom, S. Vidal, G.R. Bacanu, S.J. Elliott, M.E. Light, J.M. Herniman, G.J. Langley, M.H. Levitt and R.J. Whitby, Angew. Chem. Int. Ed. **58**, 5038 (2019). doi:10.1002/anie.201900983
[6] A. Kilaj, H. Gao, D. Rösch, U. Rivero, J. Küpper and S. Willitsch, Nat. Commun. **9**, 2096 (2018). doi:10.1038/s41467-018-04483-3
[7] A. Shugai, U. Nagel, Y. Murata, Y. Li, S. Mamone, A. Krachmalnicoff, S. Alom, R.J. Whitby, M.H. Levitt and T. Rõõm, J. Chem. Phys. **154**, 124311 (2021). doi:10.1063/5.0047350
[8] C. Beduz, M. Carravetta, J.Y.C. Chen, M. Concistrè, M. Denning, M. Frunzi, A.J. Horsewill, O.G. Johannessen, R. Lawler, X. Lei, M.H. Levitt, Y. Li, S. Mamone, Y. Murata, U. Nagel, T. Nishida, J. Ollivier, S. Rols, T. Rõõm, R. Sarkar, N.J. Turro and Y. Yang, Proc. Natl. Acad. Sci. U.S.A.**109**, 12894 (2012). doi:10.1073/pnas.1210790109
[9] K.S.K. Goh, M. Jiménez-Ruiz, M.R. Johnson, S. Rols, J. Ollivier, M.S. Denning, S. Mamone, M.H. Levitt, X. Lei, Y. Li, N.J. Turro, Y. Murata and A.J. Horsewill, Phys. Chem. Chem. Phys. **16**, 21330 (2014). doi:10.1039/C4CP03272A
[10] T.R. Huet, C.J. Pursell, W.C. Ho, B.M. Dinelli and T. Oka, J. Chem. Phys. **97**, 5977 (1992). doi:10.1063/1.463735
[11] S.S. Zhukov, V. Balos, G. Hoffman, S. Alom, M. Belyanchikov, M. Nebioglu, S. Roh, A. Pronin, G.R. Bacanu, P. Abramov, M. Wolf, M. Dressel, M.H. Levitt, R.J. Whitby, B. Gorshunov and M. Sajadi, Sci. Rep. **10**, 18329 (2020). doi:10.1038/s41598-020-74972-3
[12] A. Melentev, S. Zhukov, V. Balos, G. Hoffman, S. Alom, M. Belyanchikov, E. Zhukova, M. Dressel, G.R. Bacanu, P. Abramov, M.H. Levitt, R. Whitby, B. Gorshunov and M. Sajadi, J. Phys. Conf. Ser. **1984**, 012012 (2021). doi:10.1088/1742-6596/1984/1/012012
[13] P.M. Felker, V. Vlček, I. Hietanen, S. Fitzgerald, D. Neuhauser and Z. Bačić, Phys. Chem. Chem. Phys. **19**, 31274 (2017). doi:10.1039/C7CP06062A
[14] O. Carrillo-Bohórquez, A. Valdés and R. Prosmiti, Chem. Phys. Chem. **23**, e202200034 (2022). doi: 10.1002/cphc.202200034
[15] B. Meier, S. Mamone, M. Concistrè, J. Alonso-Valdesueiro, A. Krachmalnicoff, R.J. Whitby and M.H. Levitt, Nat. Commun. **6**, 1 (2015). doi: 10.1038/ncomms9112
[16] S. Mamone, M. Concistrè, E. Carignani, B. Meier, A. Krachmalnicoff, O.G. Johannessen, X. Lei, Y. Li, M. Denning, M. Carravetta, K. Goh, A.J. Horsewill, R.J. Whitby and M.H. Levitt, J. Chem. Phys. **140**, 194306 (2014). doi:10.1063/1.4873343
[17] M.H. Levitt, Philos. Trans. A Math. Phys. Eng. Sci. **371**, 20130124 (2013). doi: 10.1098/rsta.2012.0429
[18] Z. Bačić, V. Vlček, D. Neuhauser and P.M. Felker, Faraday Discuss. **212**, 547 (2018). doi:10.1039/C8FD00082D
[19] A. Varadwaj and P.R. Varadwaj, Chem. Eur. J. **18**, 15345 (2012). doi:10.1002/chem.201200969
[20] B. Ensing, F. Costanzo and P.L. Silvestrelli, J. Phys. Chem. A **116**, 12184 (2012). doi:10.1021/jp311161q
[21] S.P. Jarvis, H. Sang, F. Junqueira, O. Gordon, J.E.A. Hodgkinson, A. Saywell, P. Rahe, S. Mamone, S. Taylor, A. Sweetman, J. Leaf, D.A. Duncan, T.L. Lee, P.K. Thakur, G. Hoffman, R.J. Whitby, M.H. Levitt, G. Held, L. Kantorovich, P. Moriarty and R.G. Jones, Commun. Chem. **4**, 135 (2021). doi:10.1038/s42004-021-00569-0
[22] S.J. Elliott, C. Bengs, K. Kouřil, B. Meier, S. Alom, R.J. Whitby and M.H. Levitt, ChemPhysChem **19**, 251 (2018). doi:10.1002/cphc.201701330
[23] G.R. Bacanu, G. Hoffman, M. Amponsah, M. Concistrè, R.J. Whitby and M.H. Levitt, Phys. Chem. Chem. Phys. **22**, 11850 (2020). doi:10.1039/D0CP01282C
[24] E.K. Campbell, M. Holz, D. Gerlich and J.P. Maier, Nature **523**, 322 (2015). doi:10.1038/nature14566
[25] E.K. Campbell, M. Holz, J.P. Maier, D. Gerlich, G.A.H. Walker and D. Bohlender, Astrophys. J. **822**, 17 (2016). doi:10.3847/0004-637X/822/1/17
[26] E.K. Campbell and P.W. Dunk, Rev. Sci. Instrum. **90**, 103101 (2019). doi:10.1063/1.5116925
[27] A.O. Lykhin, S. Ahmadvand and S.A. Varganov, J. Phys. Chem. Lett. **10**, 115 (2018). doi:10.1021/acs.jpclett.8b03534
[28] A.S. Menon and L. Radom, J. Phys. Chem. A **112**, 13225 (2008). doi:10.1021/jp803064k
[29] S. Grimme, J. Antony, S. Ehrlich and H. Krieg, J. Chem. Phys. **132**, 154104 (2010). doi:10.1063/1.3382344
[30] L. Goerigk and S. Grimme, *Modeling of Molecular Properties* (John Wiley & Sons, Hoboken, 2011), pp. 1–16.
[31] S. Grimme, S. Ehrlich and L. Goerigk, J. Comput. Chem. **32**, 1456 (2011). doi:10.1002/jcc.21759
[32] M.J. Frisch, G.W. Trucks, H.B. Schlegel, G.E. Scuseria, M.A. Robb, J.R. Cheeseman, G. Scalmani, V. Barone, G.A. Petersson, H. Nakatsuji, X. Li, M. Caricato, A.V. Marenich, J. Bloino, B.G. Janesko, R. Gomperts, B. Mennucci, H.P. Hratchian, J.V. Ortiz, A.F. Izmaylov, J.L. Sonnenberg, D. Williams-Young, F. Ding, F. Lipparini, F. Egidi, J. Goings, B. Peng, A. Petrone, T. Henderson, D. Ranasinghe, V.G. Zakrzewski, J. Gao, N. Rega, G. Zheng, W. Liang, M. Hada, M. Ehara, K. Toyota, R. Fukuda, J. Hasegawa, M. Ishida, T. Nakajima, Y. Honda, O. Kitao, H. Nakai, T. Vreven, K. Throssell, J.A. Montgomery, Jr. J.E.

Peralta, F. Ogliaro, M.J. Bearpark, J.J. Heyd, E.N. Brothers, K.N. Kudin, V.N. Staroverov, T.A. Keith, R. Kobayashi, J. Normand, K. Raghavachari, A.P. Rendell, J.C. Burant, S.S. Iyengar, J. Tomasi, M. Cossi, J.M. Millam, M. Klene, C. Adamo, R. Cammi, J.W. Ochterski, R.L. Martin, K. Morokuma, O. Farkas, J.B. Foresman and D.J. Fox, *Gaussian16 Revision A.03* (Gaussian Inc., Wallingford, CT, 2016).

[33] F. Duschinsky, Acta Physicochim. URSS **7**, 551 (1937).

[34] C.M. Western and J. Quant, Spectrosc. Radiat. Transf. **186**, 221 (2017). doi:10.1016/j.jqsrt.2016.04.010

[35] P. Bunker and P. Jensen, *Fundamentals of Molecular Symmetry* (1st ed., CRC Press, Boca Raton, 2005), p. 101.

[36] T. Rõõm, L. Peedu, M. Ge, D. Hüvonen, U. Nagel, S. Ye, M. Xu, Z. Bačić, S. Mamone, M.H. Levitt, M. Carravetta, J.Y. Chen, X. Lei, N.J. Turro, Y. Murata and K. Komatsu, Phil. Trans. A Math. Phys. Eng. Sci. **371**, 20110631 (2013). doi: 10.1098/rsta.2011.0631